THE JOURNAL OF BIOLOGICAL CHEMISTRY
Vol. 278, No. 22, Issue of May 30, pp. 20319–20326, 2003
Printed in U.S.A.

The Dps Protein of *Agrobacterium tumefaciens* Does Not Bind to DNA but Protects It toward Oxidative Cleavage

X-RAY CRYSTAL STRUCTURE, IRON BINDING, AND HYDROXYL-RADICAL SCAVENGING PROPERTIES*

Received for publication, February 28, 2003, and in revised form, March 26, 2003
Published, JBC Papers in Press, March 26, 2003, DOI 10.1074/jbc.M302114200

Pierpaolo Ceci‡, Andrea Ilari‡, Elisabetta Falvo, and Emilia Chiancone§

From the Consiglio Nazionale delle Ricerche Institute of Molecular Biology and Pathology, Department of Biochemical Sciences "A. Rossi-Fanelli," University of Rome "La Sapienza," 00185 Rome, Italy

Agrobacterium tumefaciens **Dps (DNA-binding proteins from starved cells), encoded by the *dps* gene located on the circular chromosome of this plant pathogen, was cloned, and its structural and functional properties were determined *in vitro*. In *Escherichia coli* Dps, the family prototype, the DNA binding properties are thought to be associated with the presence of the lysine-containing N-terminal tail that extends from the protein surface into the solvent. The x-ray crystal structure of *A. tumefaciens* Dps shows that the positively charged N-terminal tail, which is 11 amino acids shorter than in the *E. coli* protein, is blocked onto the protein surface. This feature accounts for the lack of interaction with DNA. The intersubunit ferroxidase center characteristic of Dps proteins is conserved and confers to the *A. tumefaciens* protein a ferritin-like activity that manifests itself in the capacity to oxidize and incorporate iron in the internal cavity and to release it after reduction. In turn, sequestration of Fe(II) correlates with the capacity of *A. tumefaciens* Dps to reduce the production of hydroxyl radicals from H_2O_2 through Fenton chemistry. These data demonstrate conclusively that DNA protection from oxidative damage *in vitro* does not require formation of a Dps-DNA complex. *In vivo*, the hydroxyl radical scavenging activity of *A. tumefaciens* Dps may be envisaged to act in concert with catalase A to counteract the toxic effect of H_2O_2, the major component of the plant defense system when challenged by the bacterium.**

Agrobacterium tumefaciens, a soil-borne Gram-negative α-protobacterium of the family Rhizobiaceae, is the causative agent for crown gall tumor disease in more than 90 families of dicotyledonous plants resulting in major agronomic losses. Pathogenicity is due to transfer of its tumor-inducing plasmid into plant cells, where the oncogene-containing T-DNA becomes integrated into the chromosomes. This transfer system has played important roles in plant biotechnology as well as in plant molecular biology (1, 2). Recently, *A. tumefaciens* was shown to contain one circular and one linear chromosome in addition to the tumor-inducing plasmid (3), and the complete genome sequence was determined (4). Physical maps of the linear and circular chromosomal DNAs and a linkage map of the linear chromosomal DNA in *A. tumefaciens* MAFF301001 were constructed for further genome analysis (3). Chromosomally coded virulence genes were mapped exclusively on the circular chromosome.

Plant cells challenged with *A. tumefaciens* or other pathogenic microorganisms react by means of an oxidative burst that has H_2O_2 as a major component and aims at restricting the bacterial growth conditions. In turn, *A. tumefaciens* uses H_2O_2 as an intracellular and intercellular inducer for the catalase A (*katA*) gene expression. which serves to minimize the oxidative response of the infected plant cells by maintaining appropriate levels of catalase activity and H_2O_2 (5, 6).

The protection strategy against oxidative and nutritional stress has been studied extensively in *Escherichia coli* (7). A key component is a nonspecific DNA-binding protein named Dps (**D**NA-binding **p**roteins from **s**tarved cells) that protects DNA from cleavage caused by reactive oxygen species such as the hydroxyl radicals produced during oxidation of Fe(II) by H_2O_2 (8). When first described, the protective action of Dps on DNA was attributed to physical association between the two macromolecules since complex formation essentially abolishes oxidative DNA cleavage both *in vitro* and *in vivo* (8, 9). Most recently however, *E. coli* Dps was shown to possess iron and H_2O_2 detoxification capacity, and this novel property was proposed to act in concert with physical association to DNA to achieve its protection against oxidative assault (10).

The striking similarity of *E. coli* Dps with *Listeria innocua* ferritin, and in particular the presence of the unusual ferroxidase site first described in the latter protein, provide the structural basis for the ability to nullify the toxic combination of Fe(II) and H_2O_2 (12, 13). *E. coli* Dps and *Listeria* ferritin, like all members of the Dps family, are homo-polymers formed by 12 four-helix bundle subunits that assemble with 23 symmetry into a hollow shell whose cavity is about 90 Å in diameter (11, 14, 15). Relative to *Listeria* ferritin, many Dps sequences display an N-terminal extension of variable length that contains two or three positively charged lysine residues. In the *E. coli* protein, the family prototype, this N-terminal region extends from the four-helix bundle core into the solvent and is thought to play an important role in the stabilization of the complex with DNA (11). In keeping with this idea, *Listeria* ferritin (15), Dlp-1 Dlp-2 from *Bacillus anthracis* (16), HP-NAP from *Heli-*

* This work was supported by Grant "Agenzia 2000" from the Consiglio Nazionale delle Ricerche (to A. I.), and Grants "Biologia Strutturale e Dinamica di Proteine Redox" and "Centro di Eccellenza Biologia e Medicina Molecolare" from the Ministero Istruzione Università e Ricerca, and a grant from the Agenzia Spaziale Italiana (to E. C.). The costs of publication of this article were defrayed in part by the payment of page charges. This article must therefore be hereby marked "*advertisement*" in accordance with 18 U.S.C. Section 1734 solely to indicate this fact.

The atomic coordinates and structure factors (code 1O9R) have been deposited in the Protein Data Bank, Research Collaboratory for Structural Bioinformatics, Rutgers University, New Brunswick, NJ (http://www.rcsb.org/).

‡ Both authors contributed equally to the work.

§ To whom correspondence should be addressed: Consiglio Nazionale delle Ricerche Institute of Molecular Biology and Pathology, Dept. of Biochemical Sciences "A. Rossi-Fanelli," University of Rome "La Sapienza," P. Le Aldo Moro 5, 00185 Rome, Italy. Tel.: 39-6-494-0543; Fax: 39-6-444-0062; E-mail: emilia.chiancone@uniroma1.it.

cobacter pylori (17), which lack the N-terminal extension, do not bind to DNA. In contrast to the variability of the N terminus, the ferroxidase site is highly conserved. In fact, the iron ligands are part of the so-called "DNA-binding signature." The Dps ferroxidase site is unusual in that it is not embedded in a four-helix bundle as is generally the case but is shared by 2-fold symmetry-related subunits providing the iron ligands. As mentioned above, this site was first described in *Listeria* ferritin, where it is involved in the iron oxidation/incorporation process (14), which in turn is related to the iron and H_2O_2 detoxification properties of the protein (12). It is important to stress that the residues which coordinate the metal in the *Listeria* ferritin ferroxidase site have the same function in all the members of Dps family whose x-ray crystal structures have been solved so far, namely *E. coli* Dps (11), Dlp-1 Dlp-2 from *B. anthracis* (16), and HP-NAP from *H. pylori* (17). Accordingly, these proteins are endowed with the ability to oxidize and incorporate Fe(II).

In this report, we describe the cloning, x-ray crystal structure, and functional properties of *A. tumefaciens* Dps, encoded by the *dps* gene located on the circular chromosome of the bacterium. Two findings provide focus on the mechanism of DNA protection by Dps proteins. First, *A. tumefaciens* Dps does not bind DNA *in vitro* since the lysine-containing N-terminal extension, which is 11 amino acids shorter than in the *E. coli* protein, is not disordered but interacts with the four-helix bundle core. Second, *A. tumefaciens* Dps affords significant DNA protection against oxidative cleavage due to its capacity to bind iron and to inhibit hydroxyl radical formation. It follows that *in vitro* DNA protection against oxidative assault does not require formation of a Dps-DNA complex but rests on the iron binding/oxidation activity of the Dps proteins. This is the likely reason for conservation of the ferroxidase site.

EXPERIMENTAL PROCEDURES

Bacterial Strains and Media—*A. tumefaciens* strain GV3101 was grown on LB liquid medium (10 g/liters tryptone, 5 g/liters yeast extract, 5 g/liters NaCl), and LB plates containing 25 μg/ml gentamicin (Sigma), and 50 μ/ml rifampicin at 28 °C. *E. coli* strain BL21DE3 was grown at 37 °C on LB liquid medium and LB plates containing 50 μg/ml ampicillin.

Cloning of the A. tumefaciens dps Gene into the Expression Vector pet-11a—The *dps* gene was amplified by PCR from the *A. tumefaciens* GV3101 genome using primers AGR1 (5′-CAGGAGACACATATGAAGACGCACAAG-3′) and AGR2 (5′-GCTGTGTGGATCCTGTTGGAAATTC-3′). The restriction sites for *Nde*I and *Bam*HI are underlined. Isolation of the *A. tumefaciens* genomic DNA was performed using the DNeasy tissue kit (Qiagen, Chatsworth, CA). The amplified fragment (505 bp) was digested with *Nde*I and *Bam*HI, purified by the QIAquick PCR purification kit (Qiagen), and cloned subsequently into the expression vector pet-11a (Novagen) digested with *Nde*I and *Bam*HI. This plasmid was introduced into *E. coli* BL21DE3 and sequenced by *E. coli* strain BL21DE3 dideoxy sequencing to confirm the presence of the correct gene.

Expression and Purification of Dps—*E. coli* BL21DE3 cells harboring the recombinant plasmid were grown in 1 liter of liquid LB containing ampicillin (50 μg/ml) at 37 °C to an optical density of 0.6 at 600 nm. After addition of 0.5 mM isopropyl-β-D-thiogalactopyranoside to induce the transcription of the *dps* gene, the culture was incubated further for 3–4 h.

Cells were harvested (15,000 × *g* for 20 min) and suspended in 10 ml of buffer A (50 mM Tris-HCl, pH 7.5, 0.5 mM dithiothreitol, 1 mM EDTA, 500 mM NaCl) and disrupted by sonication. The lysate was centrifuged at 15,000 × *g* for 45 min. The supernatant was precipitated using two ammonium sulfate cuts at 30 and 60% saturation (w/v). At 60%, Dps remained in solution after centrifugation (15,000 × *g* for 45 min); the supernatant was dialyzed overnight against 20 mM Tris-HCl, pH 7.5, 50 mM NaCl and then loaded onto a DEAE cellulose column (DE52) equilibrated with the same buffer. Dps was eluted with 250 mM NaCl, pooled, and stored at −75 °C after controlling the purity of the preparation by Coomassie Blue staining of 15% SDS-PAGE gels.

Protein Crystallization—Crystallization was achieved at 293 K by the hanging drop vapor diffusion technique. A 2-μl volume of the protein sample, equilibrated against 30 mM Tris-HCl, pH = 7.5, 200 mM NaCl at 7 mg/ml, was mixed with an equal amount of the reservoir solution containing 0.1 M HEPES at pH values between 7.0 and 7.8 and ethylene glycol in a range between 16 and 24% v/v. Crystals grew in 1 week to about 0.5 × 0.4 × 0.2 mm^3.

TABLE I
Crystallographic data statistics

Parameters	Numerical values
Data scaling	
Data resolution (Å)	50–1.45
Completeness of data (%)	96
R_{merge} (%)	5.3
Space group	$P2_12_12$
Cell dimensions (Å)	a = 106; b = 90; c = 105.6
Refinement statistics	
R_{crys} (%)	18
R_{free} (%)	20
r.m.s.[a] deviation bonds (Å)	0.015
r.m.s. deviation angles (deg.)	2.4
Residues in most favored region of Ramachandran plot (%)	96

[a] Root mean square.

Data Collection and Processing—Data were collected as 1.0 oscillation frames using the MAR CCD detector on the x-ray beamline at ELETTRA, Basovizza (Trieste, Italy) at a wavelength of 1.2 Å. Data were collected at 100 K using 25% glycerol as cryoprotectant. The data analysis, performed with DENZO (18), indicates that the crystals are orthorhombic ($P2_12_12$) with unit cell dimensions of a = 106, b = 90.349, c = 105.6 Å. The data were scaled using SCALEPACK (18) and had an R_{sym} = 5.3% and an χ^2 = 0.97. The crystal contains six monomers/asymmetric unit, corresponding to half of the assembled molecule, with a V_M = 2.15 Å^3/Da and a solvent content of about 45%.

Structure Solution and Refinement—The structure was solved by molecular replacement using as the search probe a polyalanine-truncated model of one-half of the *E. coli* Dps dodecamer (Protein Data Bank entry 1DPS). The rotational and translational searches, performed with the program AmoRe (19) in the resolution range of 10–3.0 Å, produced a clear solution corresponding to a correlation coefficient between F_{calc} and F_{obs} of 62.0 and to an R_{fact} of 46.2%. Refinement of the atomic coordinates and displacement parameters was carried out by the maximum likelihood method with the program REFMAC (20). The refinement statistics are presented in Table I. Model building was performed using the program package XTALVIEW (21). Water molecules were added to the model manually. The final model (a hexamer) includes 972 residues (162 residues/monomer), 740 water molecules, 6 Fe(III), 2 Tris (hydroxymethyl)-aminomethane molecules, and an ethylene glycol molecule. The final R_{crys} at 1.45-Å resolution is 18%. The quality of the model was assessed by the program PROCHECK (22). The most favored regions of the Ramachandran plot contain 96.0% of non-glycine residues. The atomic coordinates and the structure factors have been deposited in the Protein Data Bank with the accession number 1O9R.

Iron Incorporation—Solutions of ferrous ammonium sulfate were prepared before each experiment by dissolving weighed amounts of the salt in AnalaR water deoxygenated by bubbling with nitrogen. The iron incorporation kinetics was monitored spectrophotometrically at 310 nm and 25 °C on a Hewlett-Packard diode array spectrophotometer after the addition of five increments of 50 Fe(II)/dodecamer to Dps solutions (1 μM) in 50 mM MOPS,[1] 200 mM NaCl, pH 7.8, equilibrated in air. The solutions were kept under continuous stirring during the course of the reaction. As a control, the rate of Fe(II) autoxidation was measured in parallel. After the incorporation of iron, the samples were subjected to gel electrophoresis under non-denaturing conditions in 7.5% (w/v) polyacrylamide gels. The gels were stained for iron with potassium ferrocyanide and for protein with Coomassie Blue.

Kinetics of Iron Release—The kinetics of iron release was measured on Dps loaded with 273 ± 40 iron atoms/dodecamer as assessed by means of the Fe(II) 2,2′-bipyridyl method (23). Sodium dithionite was used as reducing agent. Stock solutions of sodium dithionite (0.1 M) were prepared in 50 mM MOPS, pH 7.8, 200 mM NaCl under purified nitrogen gas. In the experiments, aliquots of the sodium dithionite stock solution were added by means of a gastight syringe to 1 μM Dps in the same buffer containing 4 mM 2-2′-bipyridyl. The time course of the

[1] The abbreviations used are: MOPS, 4-morpholinepropanesulfonic acid; Dpr, Dps-like peroxide resistance.

reaction was monitored at 520 nm, the wavelength corresponding to the absorption maximum of the Fe(II)-bipyridyl complex using a Hewlett-Packard diode array spectrophotometer equipped with a thermostatted cell maintained at 25 °C. The data were fitted using the program MATLAB (The Math Works Inc., Natick, MA).

Measurement of Catalase Activity—Oxygen production was measured polarographically with a Clark type O_2 electrode (Ys Model 5300 YSI) at 25 °C both in the absence and in the presence of *A. tumefaciens* or *E. coli* Dps (1 μM) in the apo or in the 24 Fe(III)-containing form. The observed traces were analyzed with the software MATLAB.

Gel Retardation Assay—Supercoiled pet-11a DNA (20 nM) was incubated with 5 μM *A. tumefaciens* or *E. coli* Dps in 20 mM MOPS (pH 7.5) for 30 min at room temperature in the presence or absence of 200 mM NaCl or 100 mM $MgCl_2$. The complexes were resolved on 1% agarose gel run in TAE buffer (0.04 M Tris acetate and 0.002 M EDTA). The gels were stained with ethidium bromide and imaged by ImageMaster VDS (Amersham Biosciences).

DNA Protection Assay—DNA protection from oxidative damage was assessed *in vitro* using pet-11a plasmid DNA (5600 bp, 20 nM), purified by a Qiaprep spin plasmid miniprep kit (Qiagen). The total reaction volume was 15 μl in 20 mM Tris-HCl, pH 7.3, 0.2 M NaCl. Plasmid DNA was allowed to interact with *A. tumefaciens* or *E. coli* Dps (5 μM) for 10 min prior to the introduction of $FeSO_4$ (50 μM) and H_2O_2 (10 mM). The reaction mixtures were incubated for 5 min at room temperature. The reactions were stopped by incubation with 2% SDS at 85 °C for 5 min. Plasmid DNA was resolved by electrophoresis on 1% agarose gel in TAE buffer. The gel was stained with ethidium bromide and imaged by ImageMaster VDS.

Protection against Hydroxyl Radical Formation—Iron-dependent hydroxyl radical formation was assayed as described by Halliwell and Gutteridge (24) and Yamamoto *et al.* (25). Fe(II) salts in solution generate hydroxyl radicals that degrade deoxyribose to a malondialdehyde-like compound that forms a chromogen with thiobarbituric acid. Fluorescence of the chromogen was used as the assay for hydroxyl radical formation. The reaction mixture contained the following reagents in a total volume of 1.2 ml at the final concentration stated: potassium phosphate buffer (10 mM, pH 7.4), NaCl (63 mM), deoxyribose (1 mM). Variable amounts of *E. coli* or A. *tumefaciens* Dps were added to the basal reaction mixture. The reaction was initiated by adding ferrous ammonium sulfate (21 μM), and the mixture was incubated at 37 °C for 15 min. Thereafter, thiobarbituric acid (1 ml at 1% w/v) plus trichloroacetic acid (1 ml at 2.8% w/v) were added. The whole was heated at 100 °C for 10 min, cooled, and the chromogen was measured by fluorescence emission at 553 nm (λ_{ex} 532 nm) using a Fluoromax fluorimeter (Spex Industry).

RESULTS

Expression and Purification of Dps—Using the amino acid sequence of *E. coli* Dps (P27430), a search of the available *A. tumefaciens* genome (www.expasy.org) revealed the presence of one Dps-like gene designated *dps* that encodes for a 162-amino-acid sequence (Fig. 1*A*). The pI and M_r values, predicted using the ProtParam program, are 5.57 and 17,823 Da, respectively, as compared with 5.78 and 18,564 Da that pertain to *E. coli* Dps. Oligonucleotides were designed based on the available nucleotide sequence. The *dps* gene was amplified by PCR, cloned into the expression vector pet-11a, and transformed into *E. coli* BL21DE3. The protein was purified to homogeneity using the two-step purification protocol described under "Experimental Procedures."

Monomer Fold and Dodecameric Assembly—The *A. tumefaciens* Dps monomer folds in the four-helix bundle typical of Dps proteins and ferritins. The four helices, A to D, are packed by hydrophobic interactions; helices B and C are connected by a long loop containing a short α-helix (BC). Twelve identical subunits assemble to form a hollow protein shell with 23 symmetry and an external diameter of 90 Å (Fig. 1*B*).

Fig. 1, *B* and *C*, shows a comparison of the *A. tumefaciens* Dps monomer with those of *E. coli* Dps and *L. innocua* ferritin, respectively. A similar comparison with the monomers of Dlp-1, Dlp-2 from *B. anthracis*, and HP-NAP from *H. pylori* is given in Fig. 1*D*. The superposition of these structures yields root mean square deviations of the Cα positions ranging from 1.2 to 1.5 Å for *A. tumefaciens* Dps relative to *L. innocua* ferritin, Dlp-1, Dlp-2, and HP-NAP, whereas the superposition between *A. tumefaciens* Dps and *E. coli* Dps results in a lower root mean square deviation, namely 0.822 Å (Fig. 1). Fig. 1 shows that the only significant differences are in the N- and C-terminal regions. Thus, the first 13–16 residues of *A. tumefaciens* Dps, which form an extension containing 3 Lys residues, are missing in the Dlp-1, Dlp-2, HP-NAP, and *L. innocua* monomers. In *E. coli* Dps, this extension is 11 residues longer than in the *Agrobacterium* protein; it is flexible (the first 9 amino acids are not visible in the x-ray crystal structure) and believed to protrude from the dodecamer and to be available for DNA binding. Surprisingly, in the *A. tumefaciens* Dps structure, the N-terminal extension is fully visible in the x-ray crystal structure as it interacts with the C terminus and with the C helix of the 3-fold symmetry-related subunit (Fig. 2). Hydrogen-bonding interactions are established by Gly^{77} through the backbone carbonyl group to Thr^3 and by Lys^5 through the backbone carbonyl to NE2 of Gln^{159}, whereas Lys^7 is hydrogen-bonded through the carbonyl oxygen to ND2 of Asn^{119} and through the backbone nitrogen to OE1 of Glu^{155}. In addition, OD1 of Asp^9 forms a salt bridge with NE of Arg^{122}.

In the structural alignment presented in Fig. 1*A*, the residues forming the so-called DNA binding signature are evidenced (in *red*). These residues comprise, as mentioned above, the iron ligands in the intersubunit ferroxidase site, namely His^{40}, His^{52}, Asp^{56}, Glu^{71}, Asp^{67}, and other residues that are likely to determine the correct fold of the iron binding site such as Trp^{41}, Gly^{45}, placed on the AB loop near His^{40}, and Gly^{77} on the first part of the CD loop near Glu^{71}. It follows that DNA binding signature is a misnomer.

A last set of residues, such as Asp^{133} and Asp^{138} (Fig. 1*A*, *green*), are at the outer rim of the hydrophilic channels along the 3-fold axes and provide the major contribution to the strongly negative electrostatic surface potential that surrounds the channels themselves to permit iron entry into the protein. Although the external electrostatic surface potential is strongly negative, positive patches like that formed by Arg^{112}, Lys^{92}, and Lys^{94} can be distinguished. They may have a role in the interaction with as yet unidentified molecular targets. As in all Dps proteins, the inner surface is strongly negative (data not shown) and is involved in the formation of the iron core.

Structural Features of the Ferroxidase Center—The $F_{obs} - F_{calc}$ difference Fourier map, calculated before the introduction of the water molecules, shows a strong peak for each monomer with a value of 8 σ placed at the interface between the 2-fold symmetry-related subunits. The peaks have been assigned to an iron ion because the peak intensity is about three times stronger than that of water molecules and because x-ray fluorescence spectra measured at ELETTRA indicated that iron atoms are present in the crystals (data not shown). If one assumes an occupancy of 0.5, the iron ions refinement gives a reasonable thermal parameter of 27 $Å^2$. The iron atom has a tetrahedral coordination sphere where two ligands are Asp^{67} and Glu^{71} of one subunit, which binds iron with side chain oxygen atoms. A third ligand is His^{40} of the 2-fold symmetry-related subunit, which binds iron with the side chain nitrogen atom (NE1), and the fourth ligand is a water molecule placed at about 3 Å from the iron ion and hydrogen-bonded to His^{52}. This iron binding site therefore closely resembles the ferroxidase site identified in the *L. innocua* dodecameric ferritin (12) that is shared by all members of the Dps family.

Since the *A. tumefaciens* Dps iron binding site is not fully occupied by the metal, the x-ray structure furnishes the unique opportunity to visualize local conformational changes induced by iron binding. Thus, two distinct conformations for the Asp^{67}

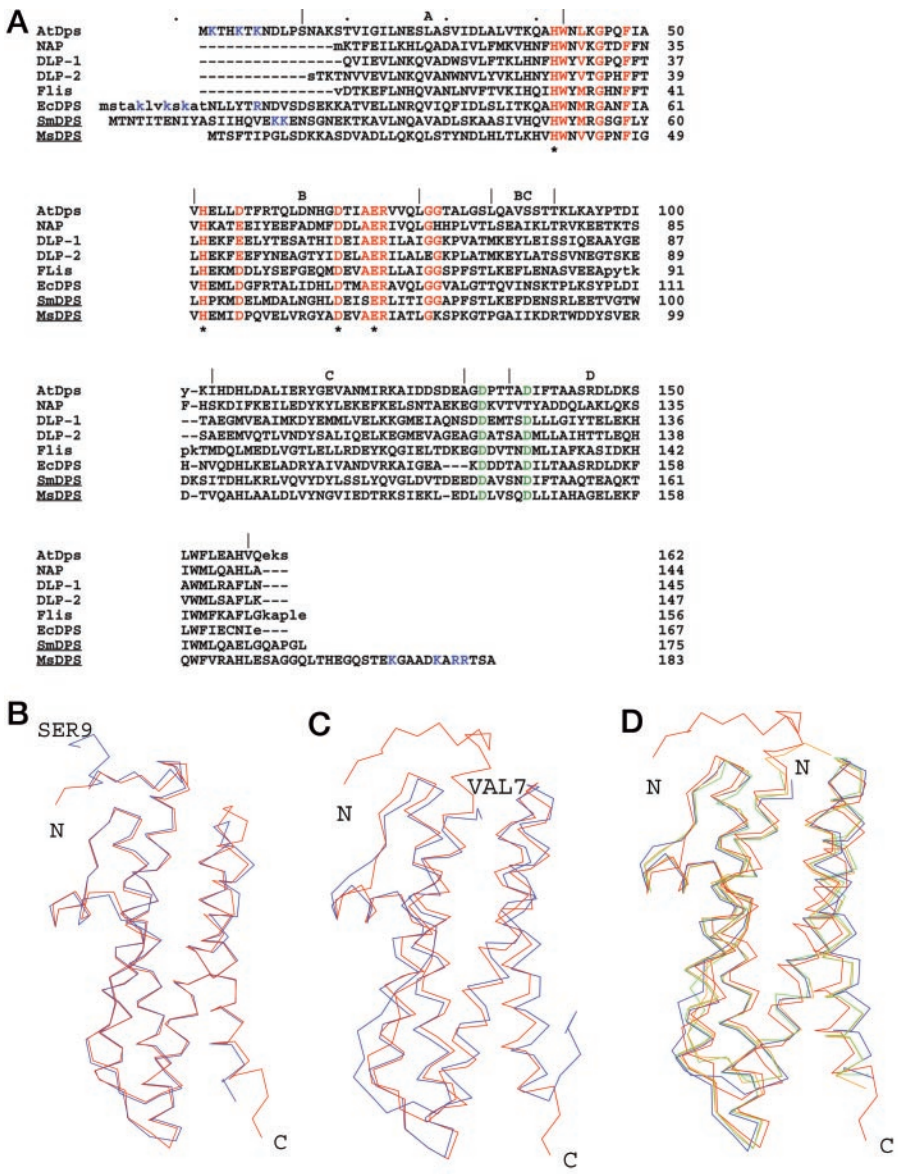

FIG. 1. **Primary structure alignment and monomer fold of Dps proteins.** *A*, alignment of Dps proteins from *A. tumefaciens* (*AtDps*), *H. pylori* (*NAP*), *B. anthracis* (*Dlp-1* and *Dlp-2*), *L. innocua* (*FLis*), *E. coli* (*EcDps*), *S. mutans* (*SmDps*), and *M. smegmatis* (*MsDps*). The residues of the so-called DNA binding signature are depicted in *red*, those lining the pore along the 3-fold axes are in *green*, and the positively charged ones at the N or C terminus are in *blue*. The amino acids of the ferroxidase center are indicated with *asterisks*. *B–D*, structural overlays of the monomer fold of Dps proteins. *B*, superposition of the Cα traces of *A. tumefaciens* Dps in *red* and *E. coli* Dps in *blue*; *C*, superposition of the Cα traces of *A. tumefaciens* Dps in *red* and *L. innocua* ferritin in *blue*; *D*, superposition of the Cα traces of *A. tumefaciens* Dps in *red*, *H. pylori* NAP in *blue*, *B. anthracis* Dlp-1 and Dlp-2 in *green* and *orange*, respectively. The overlay was obtained using the program SEQUOIA (33) and was generated with the program MOLSCRIPT (34).

side chain are apparent in the $2F_{obs} - F_{calc}$ electron density map (Fig. 3). When the site is empty, Asp^{67} assumes a rotameric conformation that allows formation of a salt bridge with Lys^{37} rather than coordination of the iron.

Iron Incorporation and Release—In accordance with the presence of the ferroxidase site, *A. tumefaciens* Dps is able to oxidize and incorporate iron. This is indicated by electrophoretic analysis of the products obtained upon incubation with ferrous iron in the presence of molecular oxygen in 50 mM MOPS, 200 mM NaCl, pH 7.8 (data not shown). A progress curve of iron uptake by *A. tumefaciens* Dps is shown in Fig. 4*A*; the half-time observed upon addition of 100 Fe/molecule corresponds to 27.7 s. Similar values were obtained with *E. coli* Dps under the same experimental conditions (data not shown).

As for *Listeria* ferritin (12, 14) and for all Dps proteins tested (10, 15, 25, 26), up to 400–500 Fe(II) can be loaded into the protein cavity. The iron-loaded protein was used to follow the kinetics of iron reduction, which results in the release of the metal into the solvent. For comparative purposes, dithionite was used as the reducing agent, and iron release was followed by measuring formation of the Fe(II) complex with 2-2′-bipyridyl at 520 nm. The time course of the reaction is biphasic with kinetic constants of 0.85×10^{-2} s^{-1} and 7.4×10^{-4} s^{-1} at a pH of 7.8 (Fig. 4*B*). The fast phase accounts for about 70% of the total absorbance change. This behavior resembles that of *E. coli* Dps, which releases iron with a biphasic process with rate constants 4.7×10^{-2} and 12×10^{-4} s^{-1} (13). A 2-fold variation of the bipyridyl concentration does not change the observed rates, indicating that formation of the $Fe(bipyridyl)^{2+}{}_3$ complex is rapid compared with the iron reduction/release process.

Measurement of Catalase Activity—The catalase activity of *A. tumefaciens* Dps was tested in 50 mM MOPS, 200 mM NaCl, pH 7.5 and was compared with that of *E. coli* Dps. The O_2 evolution measured by electrode oximetry after addition of 80

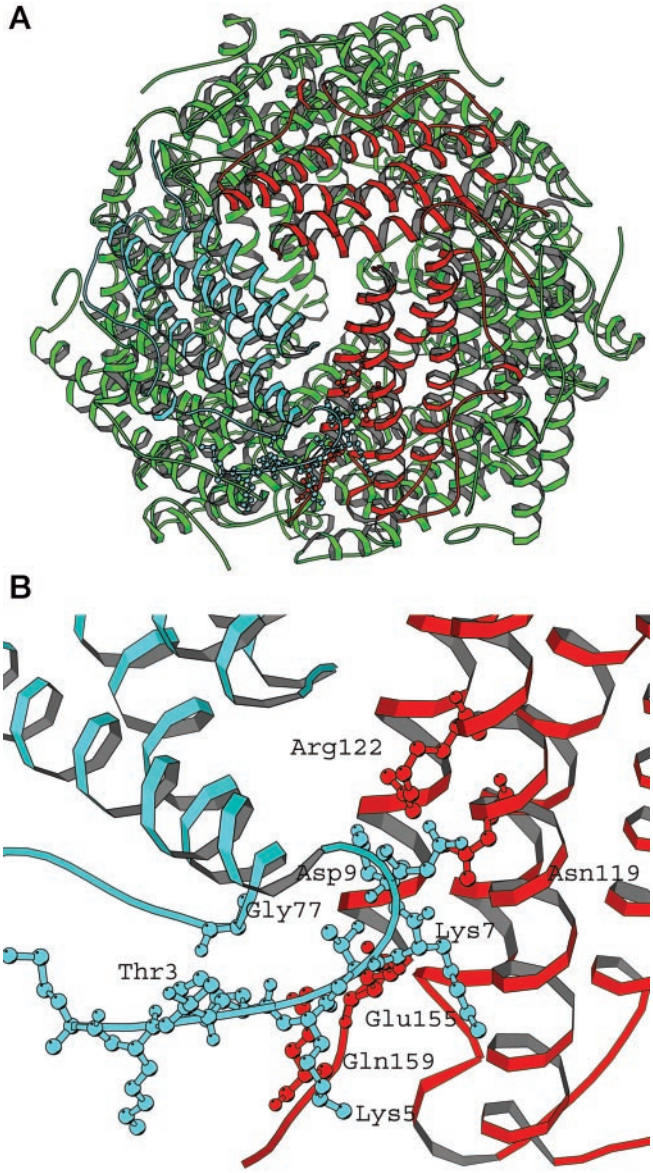

FIG. 2. **X-ray crystal structure of the *A. tumefaciens* Dps dodecamer.** *A*, view along a 3-fold symmetry axis. *B*, blowup of the N terminus (in *light blue*) showing the interactions established with the C terminus and the C helix of the 3-fold symmetry-related subunit (in *red*).

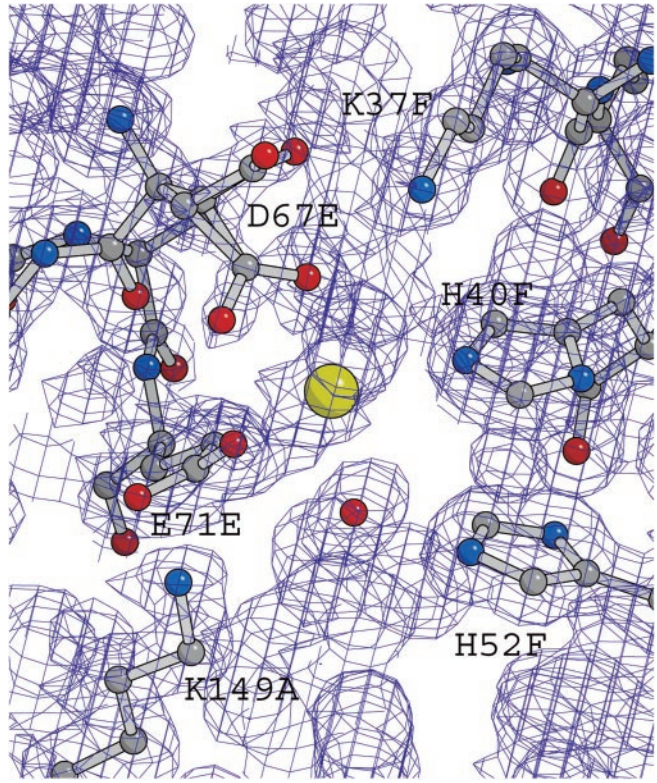

FIG. 3. **Electron density map of the ferroxidase center in *A. tumefaciens* Dps.** The ferroxidase center residues (Asp^{67}, Glu^{71} from subunit E, His^{40} and His^{52} from subunit F) and neighboring residues (Lys^{37} from subunit F and Lys^{149} from subunit A) are indicated. The iron atom is shown in *yellow*, and a water molecule is depicted in *red*. The $2F_{obs} - F_{calc}$ electron density map clearly shows two distinct conformations for the Asp^{67} side chain. The picture was generated with BOBSCRIPT (35).

μM H_2O_2 to a 1 μM solution of *A. tumefaciens* Dps containing 24 Fe(III)/molecule did not differ significantly from that measured with buffer alone. The *E. coli* Dps control analyzed in parallel displayed the same activity reported by Zhao *et al.* (10), *i.e.* 1 mol of Dps containing 24 Fe(III)/molecule disproportionates 0.12 ± 0.03 mol H_2O_2.

DNA Binding Capacity Assayed in Gel Retardation Assays—The binding of *A. tumefaciens* Dps to DNA was analyzed *in vitro* by studying complex formation in agarose electrophoresis experiments (Fig. 5). Dps-DNA complexes were not detected when purified Dps (5 μM) was added to 20 nM supercoiled pet-11a DNA in 20 mM MOPS (pH 7.5) in the presence or absence of 200 mM NaCl or 100 mM $MgCl_2$. *E. coli* Dps analyzed in parallel gives rise to a complex with DNA that does not enter the gel in accordance with previous results (8). The same results were obtained in another set of experiments in which the Dps concentration was increased 10-fold while keeping DNA constant (data not shown).

DNA Protection against Hydroxyl Radical Formation—Dps proteins afford protection of DNA from cleavage due to radicals produced in Fe(II)-mediated Fenton reactions, a property attributed originally to physical association between the two macromolecules (8). To establish whether *A. tumefaciens* Dps is able to protect DNA although complex formation is not apparent in the gel retardation assays just presented, an *in vitro* DNA damage assay was set up. The combined effect of 50 μM Fe(II) and 10 mM H_2O_2 on the integrity of plasmid pet-11a (5600 bp) was assessed in the presence and absence of Dps. *E. coli* Dps was used as a control. Under the conditions employed, DNA is fully degraded, and either *E. coli* or *A. tumefaciens* Dps yields essentially complete protection (Fig. 6).

In a different type of experiment, iron-dependent hydroxyl radical formation in the presence or absence of *A. tumefaciens* or *E. coli* Dps was investigated using the fluorimetric assay (24, 25) described under "Experimental Procedures." Addition of *E. coli* or *A. tumefaciens* Dps inhibits efficiently hydroxyl radical formation. The extent of inhibition varies from 55 to 70% depending on the Dps to Fe(II) molar ratio (Table II).

DISCUSSION

The present work on *A. tumefaciens* Dps brings into a new focus the structure-function relationships in the Dps family. It shows that the possible interaction between a given Dps protein with DNA may not be predictable based on simple sequence analysis of the N terminus. More importantly, it demonstrates that formation of Dps-DNA complex(es) is not a prerequisite for the protection of DNA against oxidative cleavage *in vitro*.

The current thinking on the interaction between Dps proteins and DNA rests heavily on the behavior of *E. coli* where it

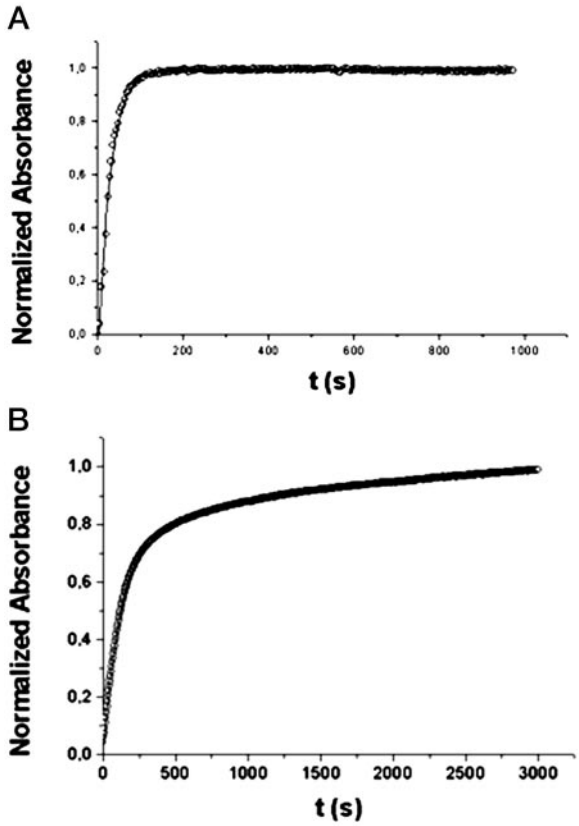

FIG. 4. **Kinetics of the iron oxidation/incorporation and reduction/release processes in *A. tumefaciens* Dps.** *A*, iron oxidation/incorporation kinetics monitored spectrophotometrically at 310 nm and 25 °C after the addition of 200 Fe(II)/dodecamer to a 1 μM Dps solution in 50 mM MOPS-HCl, 200 mM NaCl, pH 7.8, equilibrated in air. *B*, iron reduction/release kinetics performed in the presence of 2-2′ bipyridyl using 100 mM sodium dithionite as reducing agent in 50 mM MOPS-HCl, pH 7.8. The concentration of Dps loaded with 274 iron atoms was 1 μM. Formation of the $Fe(bipyridyl)^{2+}_3$ complex was followed at 520 nm.

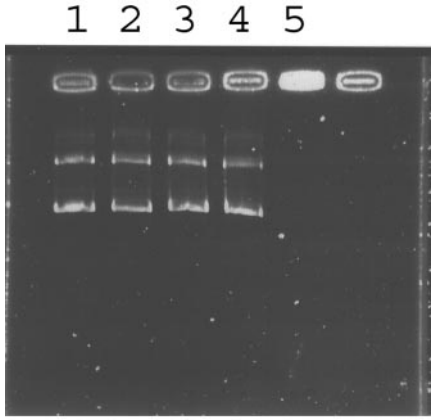

FIG. 5. **Gel retardation assays on mixtures of *A. tumefaciens* Dps and DNA.** Supercoiled pet-11a DNA (20 nM) was incubated with 5 μM *E. coli* or *A. tumefaciens* Dps in 20 mM MOPS-HCl (pH 7.5) in the presence or absence of 200 mM NaCl or 100 mM $MgCl_2$ and resolved in 1% agarose gel run in TAE buffer. *Lane 1*, native plasmid DNA. *Lane 2*, plasmid DNA with *A. tumefaciens* Dps. *Lane 3*, plasmid DNA with *A. tumefaciens* Dps in the presence of 200 mM NaCl. *Lane 4*, plasmid DNA with *A. tumefaciens* Dps in the presence of 100 mM $MgCl_2$. *Lane 5*, plasmid DNA with *E. coli* Dps.

results in the rapid formation of highly ordered and tightly packed Dps-DNA co-crystals (9). Since such structures have been detected in the cytoplasm of starved bacteria, they have been proposed to be a general mode of DNA protection based on

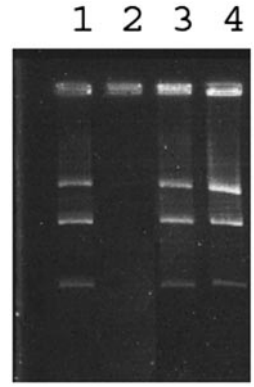

FIG. 6. **DNA protection by *A. tumefaciens* Dps. All reaction mixtures contained 20 nM pet-11a.** *Lane 1*, native plasmid DNA. *Lane 2*, plasmid DNA exposed to 50 μM $FeSO_4$ and then exposed to 10 mM H_2O_2. *Lane 3*, plasmid DNA with 5 μM *A. tumefaciens* Dps exposed to 50 μM $FeSO_4$ and then exposed to 10 mM H_2O_2. *Lane 4*, plasmid DNA with 5 μM *E. coli* Dps exposed to 50 μM $FeSO_4$ and then exposed to 10 mM H_2O_2.

TABLE II
Effect of A. tumefaciens Dps and E. coli Dps on Fe(II)-dependent hydroxyl radical formation

	Dps Concentration	Inhibition[a]
	mM	*%*
A. tumefaciens Dps	50	50.7 ± 2.0
	200	65.3 ± 1.8
	400	67.3 ± 1.0
E. coli Dps	50	51.8 ± 3.5
	200	68.3 ± 2.4
	400	71.1 ± 2.1

[a] The values are the mean ± standard deviation for experiments carried out in triplicate

its physical sequestration by Dps (8). The DNA binding ability of *E. coli* Dps has been associated to the presence of a flexible, disordered N-terminal tail containing three positively charged lysine residues and one arginine residue that can hook the negatively charged DNA backbone (11). Therefore, the positively charged N-terminal extension of *A. tumefaciens* Dps, albeit 11 residues shorter than in the *E. coli* protein, was expected to confer DNA binding capacity to this member of the family. However, there is no evidence of complex formation with DNA in band shifts experiments such as those presented in Fig. 5. This unforeseen behavior is explained by the x-ray crystal structure. In *A. tumefaciens* Dps, the N terminus is not disordered as in the *E. coli* protein but is blocked onto the four-helix bundle of the 3-fold symmetry-related subunit by several interactions that involve the backbone carbonyl oxygen and peptide nitrogen atoms of Thr^3, Lys^5, and Lys^7 and one salt bridge established by Asp^9 with Arg^{122} (Fig. 2).

The behavior of *A. tumefaciens* Dps therefore indicates that an effective interaction of the Dps with DNA requires the positively charged N terminus to be disordered and endowed with flexibility. In line with this contention, the absence of the first N-terminal residues in *Listeria* ferritin, *B. anthracis* Dpl-1 and Dpl-2, and HP-NAP correlates beautifully with their inability to form a complex with DNA (15–17), whereas the short, two-lysine-containing N terminus of *B. subtilis* MrgA accounts for its binding to DNA (27). In *Streptococcus mutans*, the Dpr (**D**ps-like **p**eroxide **r**esistance) protein does not interact with DNA in accordance with the presence of a long N-terminal tail that does not contain positively charged residues apart from two lysines located near the predicted beginning of the A helix (25). Of interest is the formation of a Dps-DNA complex by *Mycobacterium smegmatis* Dps (28). This protein has a truncated, uncharged N terminus but contains an unusually long C

terminus with 3 lysine and 2 arginine residues that thus is able to substitute the N terminus in the interaction with DNA (Fig. 1*A*). The behavior of Dps from *Synechococcus sp.* strain PCC 7942 remains unexpected. This heme-binding Dps-like protein is reported to bind DNA (29). However, the long N terminus does not contain lysine or arginine residues, and there is no C-terminal extension (Fig. 1*A*).

Despite the inability to bind DNA, *A. tumefaciens* Dps protects it from oxidative damage due to the ferritin-like activity that has its structural basis in the ferroxidase center. This contains the two canonical metal binding sites (A and B) required for the formation of an oxo-bridged intermediate during oxidation reaction but has an unusual intersubunit location as described first in *L. innocua* ferritin (15). In *A. tumefaciens* Dps, the A site is occupied partially by iron, which is coordinated by Asp^{67} and Glu^{71} from one subunit and His^{40} from the 2-fold symmetry-related one, whereas the B site is occupied by a water molecule that is hydrogen-bonded to His^{52}. In all known ferroxidase centers, the A and B sites have different affinities for the metal. In the x-ray structures of Dps proteins reported so far, site B contains a water molecule due to the lower affinity for iron, whereas site A is either totally or partially occupied by the metal or contains a water molecule. Thus, in *Listeria* ferritin (15), HP-NAP from *H. pylori*, and Dlp-1 and Dlp-2 from *B. anthracis* site A contains iron (16, 17), whereas in *E. coli* Dps, a water molecule is in place of the metal even in crystals of the iron-loaded protein (13). According to Ilari *et al.* (15), the A site affinity is influenced by the nature and spatial arrangement of the residues surrounding the iron-coordinating ligands. Thus, the lower affinity of the A site in *E. coli* Dps relative to *Listeria* ferritin and the other Dps proteins just mentioned can be ascribed to the replacement of a histidine residue (His^{28} in *Listeria* ferritin) with a lysine residue (Lys^{48}) that engages one of the iron-coordinating ligands (Glu^{62}) in a salt bridge. The differences in the residues surrounding the ferroxidase site may be reflected also in the different catalase activity observed in *E. coli* and *A. tumefaciens* Dps.

The partial occupancy of the A site by iron in *A. tumefaciens* Dps offers the unique opportunity to visualize the conformational changes induced by iron binding in the ferroxidase center itself. The electron density map shows that Asp^{67} can adopt two configurations: in one, it coordinates iron, and the site architecture resembles that of *L. innocua* ferritin (15), and in the other, it forms a salt bridge with Lys^{37}, and the site architecture resembles that of *E. coli* Dps (Fig. 3).

The similarity of the ferroxidase centers in all members of the Dps family has its functional manifestation in the similarity of the iron oxidation/incorporation and release processes. Thus, all Dps proteins tested are able to oxidize and incorporate up to 400–500 iron ions in their internal cavity and to release them after reduction. Further, the kinetic features of both reactions are close to each other. The ferritin-like activity of Dps proteins has yet another facet of major biological relevance, namely the capacity to counteract the toxic action of H_2O_2, a common component of the defense systems put into action when organisms, including plants, are challenged by pathogenic bacteria. DNA damage in particular is due to the concerted action of H_2O_2 and Fe(II), which generates hydroxyl radicals through Fenton chemistry. In turn, these radicals cause DNA strand breaks by oxidizing the sugar and base moieties. As in the case of *E. coli* Dps (10) and *S. mutans* Dpr (25), *A. tumefaciens* Dps reduces significantly the production of hydroxyl radicals generated by Fenton chemistry i*n vitro* (Table II) and thus preserves the integrity of plasmid pet-11a (Fig. 6). Interestingly, the protective effect against oxidative damage does not appear to depend on the formation of a Dps-DNA complex as it is of very similar magnitude in *A. tumefaciens* and *E. coli* Dps, although the former protein does not interact with DNA. It follows that *in vitro* DNA protection by Dps proteins does not require the physical sequestration of DNA as hitherto believed but can be attributed solely to their Fe(II) scavenging capacity.

A number of experiments indicates that also *in vivo*, the Fe(II) capacity of Dps proteins is the major player in affording DNA protection against oxidative stress. Thus, in *Campylobacter jejuni*, where Dps is expressed constitutively, a Dps-deficient mutant was found to be more vulnerable to H_2O_2 than the parental strain, and the iron chelator Desferal was observed to restore H_2O_2 resistance (30). It should be stressed that *C. jejuni* Dps is not likely to interact with DNA since it lacks the two known interacting modules, namely the N- and C-terminal extension. Another example is furnished by *S. mutans* where Dpr protects cells from peroxides and confers aerotolerance (31) in accordance with the inhibition of iron-dependent hydroxyl radical formation *in vitro* (25). As in the case of *C. jejuni* Dps, *S. mutans* Dpr does not bind DNA (25). On the basis of these data, *A. tumefaciens* Dps is expected to play a significant role *in vivo* when the bacterium has to face the production of H_2O_2 by the infected plant. Dps can act in concert with catalase A in the elimination of the toxic effects of H_2O_2 by removing Fe(II) from the intracellular medium and thereby inhibiting the generation of the DNA-damaging hydroxyl radicals. It remains to be established whether the DNA binding capacity of Dps proteins such as *E. coli* Dps (8, 9) may serve an additional, specific regulatory role in the bacterium, as suggested by the highly pleiotropic phenotype of mutant cells lacking Dps with respect to the proteins synthesized during prolonged starvation (32).

In conclusion, the *in vitro* characterization of the structural and functional properties of *A. tumefaciens* Dps provides a deeper understanding of the DNA-protective action exerted by the members of the Dps family. It shows unequivocally that the Fe(II) binding ability of these proteins suffices to prevent the adverse effects of Fenton chemistry and thereby provides a molecular explanation for the conservation of their characteristic intersubunit ferroxidase site.

REFERENCES

1. Klee, H., Horsch, R., and Rogers, S. (1987) *Annu. Rev. Plant Physiol.* **38,** 467–486
2. Zupan, J., and Zambrynski, P. (1997) *Crit. Rev. Plant Sci.* **16,** 279–295
3. Suzuki, K., Iwata, K., and Yoshida, K. (2001) *DNA Res.* **8,** 141–152
4. Wood, D. W., Setubal, J. C., Kaul, R., Monks, D. E., Kitajima, J. P., Okura, V. K., Zhou, Y., Chen, L., Wood, G. E., Almeida, N. F., Jr., Woo, L., Chen, Y., Paulsen, I. T., Eisen, J. A., Karp, P. D., Bovee, D., Sr., Chapman, P., Clendenning, J., Deatherage, G., Gillet, W., Grant, C., Kutyavin, T., Levy, R., Li, M.-J., McClelland, E., Palmieri, A., Raymond, C., Rouse, G., Saenphimmachak, C., Wu, Z., Romero, P., Gordon, D., Zhang, S., Yoo, H., Tao, Y., Biddle, P., Jung, M., Krespan, W., Perry, M., Gordon-Kamm, B., Liao, L., Kim, S., Hendrick, C., Zhao, Z.-Y., Dolan, M., Chumley, F., Tingey, S. V., Tomb, J.-F., Gordon, M. P., Olson, M. V., and Nester, E. W. (2001) *Science* **294,** 2317–2323
5. Xu, X. Q., Li, L. P., and Pan, S. Q. (2001) *Mol. Microbiol.* **42,** 645–657
6. Storz, G., and Imlay, J. A. (1999) *Curr. Opin. Microbiol.* **2,** 188–194
7. Dukan, S., and Nyström, T. (1999) *J. Biol. Chem.* **274,** 26027–26032
8. Martinez, A., and Kolter, R. (1997) *J. Bacteriol.* **179,** 5188–5194
9. Wolf, S. G., Frenkiel, D., Arad, T., Finkel, S. E., Kolter, R., and Minsky, A. (1999) *Nature* **400,** 83–85
10. Zhao, G., Ceci, P., Ilari, A., Giangiacomo, L., Laue, T. M., Chiancone, E., and Chasteen, N. D. (2002) *J. Biol. Chem.* **277,** 27689–27696
11. Grant, R. A., Filman, D. J., Finkel, S. E., Kolter, R., and Hogle, J. M. (1998) *Nat. Struct. Biol.* **5,** 294–303
12. Yang, X., Chiancone, E., Stefanini, S., Ilari, A., and Chasteen, N. D. (2000) *Biochem. J.* **349,** 783–786
13. Ilari, A., Ceci, P., Ferrari, D., Rossi, G. L., and Chiancone, E. (2002) *J. Biol. Chem.* **277,** 37619–37623
14. Bozzi, M., Mignogna, G., Stefanini, S., Barra, D., Longhi, C., Valenti, P., and Chiancone E. (1997) *J. Biol. Chem.* **272,** 3259–3265
15. Ilari, A., Stefanini, S., Chiancone, E., and Tsernoglou, D. (2000) *Nat. Struct. Biol.* **7,** 38–43
16. Papinutto, E., Dundon, W. G., Pitulis, N., Battistutta, R., Montecucco, C., and Zanotti, G. (2002) *J. Biol. Chem.* **277,** 15093–15098
17. Zanotti, G., Papinutto, E., Dundon, W. G., Battistutta, R., Seveso, M., Del

Giudice, G., Rappuoli, R., and Montecucco, C. (2002) *J. Mol. Biol.* **323,** 125–130
18. Ottwinowski, Z., and Minor, W. (1997) *Methods Enzymol.* **276,** 307–326
19. Navaza, J. (1994) *Acta Crystallogr. Sect. A* **50,** 157–163
20. Murshudov, G. N., Lebedev, A., Vagin, A., Wilson, K. S., and Dodson, E. J. (1999) *Acta Crystallogr. Sect. D Biol. Crystallogr.* **55,** 247–255
21. McRee, D. E. (1993) *Practical Protein Crystallography*, pp. 365–374, Academic Press, Orlando, FL
22. Laskowski, R. A., McArthur, M. W., Moss, D. S., and Thornton, J. M. (1993) *J. Appl. Crystallogr.* **26,** 283–291
23. Botwell, T. H., and Mallet, B. (1955) *Biochem. J.* **59,** 599–602
24. Halliwell, B., and Gutteridge, J. M. (1981) *FEBS Lett.* **128,** 347–352
25. Yamamoto, Y., Poole, L. B., Hantgan, R. R., and Kamio, Y. (2002) *J. Bacteriol.* **184,** 2931–2939
26. Tonello, Dundon, W. G., Satin, B., Molinari, M., Tognon, G., Grandi, G., Del Giudice, G., Rappuoli, R., and Montecucco, C. (1999) *Mol. Microbiol.* **34,** 238–246
27. Chen, L., and Helmann, J. D. (1995) *Mol. Microbiol.* **18,** 295–300
28. Gupta, S., Pandit, S. B., Srinivasan, N., and Chatterji, D. (2002) *Protein Eng.* **15,** 503–511
29. Pena, M. M. O., and Bullerjahn, G. S. (1995) *J. Biol. Chem.* **38,** 22478–22482
30. Ishikawa, T., Yoshimitsu, M., Kawabata, S., Takade, A., Harada, M., Wai, S. N., and Yoshida, S. (2003) *J. Bacteriol.* **185,** 1010–1017
31. Yamamoto, Y., Poole, L. B., Higuchi, M., and Kamio, Y. (2000) *J. Bacteriol.* **182,** 3740–3747
32. Almiron, M., Link, A. J., Deirdre, F., and Kolter, R. (1992) *Genes Dev.* **6,** 2646–2654
33. Bruns, C. M., Hubatsch, I., Ridderström, M., Mannervik, B., and Tainer, J. A. (1999) *J. Mol. Biol.* **288,** 427–439
34. Kraulis, P. J. (1991) *J. Appl. Crystallogr.* **24,** 946–950
35. Esnouf, R. M. (1999) *Acta Crystallogr. Sect. D Biol. Crystallogr.* **55,** 938–940

The Dps Protein of *Agrobacterium tumefaciens* Does Not Bind to DNA but Protects It toward Oxidative Cleavage: X-RAY CRYSTAL STRUCTURE, IRON BINDING, AND HYDROXYL-RADICAL SCAVENGING PROPERTIES

Pierpaolo Ceci, Andrea Ilari, Elisabetta Falvo and Emilia Chiancone

J. Biol. Chem. 2003, 278:20319-20326.
doi: 10.1074/jbc.M302114200 originally published online March 26, 2003
